Hybrid III–V/silicon laser with laterally coupled Bragg grating

Yu-Lian Cao,[1,2,5] Xiao-Nan Hu,[1,5] Xian-Shu Luo,[3] Jun-Feng Song,[3] Yuanbing Cheng,[1] Cheng-Ming Li,[1] Chong-Yang Liu,[1] Hong Wang,[1] Liow Tsung-Yang,[3] Guo-Qiang Lo,[3] and QiJie Wang[1,4*]

[1]*OPTIMUS, Photonics Center of Excellence, School of Electrical & Electronic Engineering, Nanyang Technological University, 50 Nanyang Ave, 639798, Singapore*

[2]*Nano-Optoelectronics Laboratory, Institute of Semiconductors, Chinese Academy of Sciences, 35 Qinghua East Road A, Beijing, 100083, China*

[3]*Institute of Microelectronics, A*STAR, 11 Science Park Road, 117685, Singapore*

[4]*The Centre for Disruptive Photonic Technology, School of Physical and Mathematical Sciences, Nanyang Technological University, Singapore, 50 Nanyang Ave,63737, Singapore*

[5]*These authors contributed equally to this work*

**qjwang@ntu.edu.sg;*

Abstract: In this paper, we demonstrate a compact electrically pumped distributed-feedback hybrid III–V/silicon laser with laterally coupled Bragg grating for the first time to the best of our knowledge. The hybrid laser structure consists of AlGaInAs/InP multi-quantum-well gain layers on top of a laterally corrugated silicon waveguide patterned on a silicon on insulator (SOI) substrate. A pair of surface couplers is integrated at the two ends of the silicon waveguide for the optical coupling and characterization of the ouput light. Single wavelength emission of ~1.55µm with a side-mode-suppression- ratio larger than 20dB and low threshold current density of 1.54kA/cm^2 were achieved for the device under pulsed operation at 20 °C.

OCIS codes: (250.5960) Semiconductor lasers; (250.5300) Photonic integrated circuits; (140.3490) Lasers, distributed-feedback.

References and links

1. R. Soref, "The past, present and future of silicon photonics," IEEE J. Sel. Top. Quantum Electron. **12**(6), 1678–1687 (2006).
2. A. W. Fang, H. Park, O. Cohen, R. Jones, M. J. Paniccia, and J. E. Bowers, "Electrically pumped hybrid AlGaInAs-silicon evanescent laser," Opt. Express **14**(20), 9203–9210 (2006).
3. A. W. Fang, R. Jones, H. Park, O. Cohen, O. Raday, M. J. Paniccia, and J. E. Bowers, "Integrated AlGaInAs-silicon evanescent race track laser and photodetector," Opt. Express **15**(5), 2315–2322 (2007).
4. A. W. Fang, E. Lively, Y.-H. Kuo, D. Liang, and J. E. Bowers, "A distributed feedback silicon evanescent laser," Opt. Express **16**(7), 4413–4419 (2008).
5. S. Keyvaninia, G. Roelkens, D. Van Thourhout, C. Jany, M. Lamponi, A. Le Liepvre, F. Lelarge, D. Make, G.-H. Duan, D. Bordel, and J.-M. Fedeli, "Demonstration of a heterogeneously integrated III-V/SOI single wavelength tunable laser," Opt. Express **21**(3), 3784–3792 (2013).
6. S. Stankovic, R. Jones, M. N. Sysak, J. M. Heck, G. Roelkens, and D. V. Thourhout, "Hybrid III–V/Si distributed-feedback laser based on adhesive bonding," IEEE Photon. Technol. Lett. **24**(23), 2155–2158 (2012).
7. J. Buus and E. J. Murphy, "Tunable lasers in optical networks," J. Lightwave Technol. **24**(1), 5–11 (2006).
8. M. Seimetz, "Laser linewidth limitations for optical systems with high-order modulation employing feed forward digital carrier phase estimation," Proc. of the Opt. Fiber Commun. Conf., San Diego, CA, USA, 2008, Paper OtuM2.
9. H. Ishii, K. Kasaya, and H. Oohashi, "Spectral linewidth reduction in widely wavelength tunable DFB laser array," IEEE J. Sel. Top. Quantum Electron. **15**(3), 514–520 (2009).
10. S. Srinivasan, N. Julian, J. Peters, D. Liang, and J. E. Bowers, "Reliability of hybrid silicon distributed feedback lasers," IEEE J. Sel. Top. Quantum Electron. **19**(4), 1501305 (2013).
11. R. D. Martin, S. Forouhar, S. Keo, R. J. Lang, R. G. Hunspreger, R. Tiberio, and P. F. Chapman, "CW performance of an InGAs-GaAs-AlGaAs laterally-coupled distributed feedback (LC-DFB) ridge laser diode," IEEE Photon. Technol. Lett. **7**(3), 244–246 (1995).

#232468 - $15.00 USD Received 13 Jan 2015; revised 14 Mar 2015; accepted 16 Mar 2015; published 30 Mar 2015

12. O. Bondarenko, Q. Gu, J. Shane, A. Simic, B. Slutsky, and Y. Fainman, "Wafer bonded distributed feedback laser with sidewall modulated Bragg gratings," Appl. Phys. Lett. **103**(4), 043105 (2013).
13. A. Laakso, J. Karinen, and M. Dumitrescu, "Modeling and design particularities for distributed feedback lasers with laterally-coupled ridge-waveguide surface gratings," Proc. SPIE **7933**, 79332 (2011).
14. A. Laakso, M. Dumitrescu, J. Viheriälä, J. Karinen, M. Suominen, and M. Pessa, "Optical modeling of laterally-corrugated ridge-waveguide gratings," Opt. Quantum Electron. **40**(11-12), 907–920 (2008).
15. P. Yeh and A. Yariv, Optical Waves in Crystals: *Propagation and Control of Laser Radiation* (John Wiley and Sons, 2003), pp. 560–575.
16. R. M. Briggs, C. Frez, M. Bagheri, C. E. Borgentun, J. A. Gupta, M. F. Witinski, J. G. Anderson, and S. Forouhar, "Single-mode 2.65 µm InGaAsSb/AlInGaAsSb laterally coupled distributed-feedback diode lasers for atmospheric gas detection," Opt. Express **21**(1), 1317–1323 (2013).
17. L. A. Coldren and S. W. Corzine, *Diode Lasers and Photonic Integrated Circuits* (Wiley, 1995), Chap. 2.
18. S. Keyvaninia, S. Verstuyft, L. Van Landschoot, F. Lelarge, G.-H. Duan, S. Messaoudene, J. M. Fedeli, T. De Vries, B. Smalbrugge, E. J. Geluk, J. Bolk, M. Smit, G. Morthier, D. Van Thourhout, and G. Roelkens, "Heterogeneously integrated III-V/silicon distributed feedback lasers," Opt. Lett. **38**(24), 5434–5437 (2013).
19. S. Srinivasan, A. W. Fang, D. Liang, J. Peters, B. Kaye, and J. E. Bowers, "Design of phase-shifted hybrid silicon distributed feedback lasers," Opt. Express **19**(10), 9255–9261 (2011).
20. Y. Zhang, H. Qu, H. Wang, S. Zhang, L. Liu, S. Ma, and W. Zheng, "A hybrid silicon single mode laser with a slotted feedback structure," Opt. Express **21**(1), 877–883 (2013).
21. A. Mekis, S. Gloeckner, G. Masini, A. Narasimha, T. Pinguet, S. Sahni, and P. De Dobbelaere, "A gratingcoupler-enabled CMOS photonics platform," IEEE J. Sel. Top. Quantum Electron. **17**(3), 597–608 (2011).

1. Introduction

With the advances of CMOS technology, compact and low cost active optical devices including modulators and detectors have been achieved on the silicon-on-insulator (SOI) platform, whereas the practical electrically pumped light source on this platform is still missing due to the lack of efficient light generation from silicon-based materials [1]. Recently, new hybrid integration architectures of epitaxial III-V layer on silicon have been developed by wafer bonding techniques to fulfill the demand of electrically pumped lasers in silicon photonic integrated circuits [2]. Such a hybrid structure exploits the highly efficient light emission properties of direct bandgap III–V semiconductor materials.

Several configurations of single-wavelength lasers have been demonstrated for optical communication in the last several years using this hybrid integration structure based on distributed feedback (DFB) or distributed Bragg reflector (DBR) geometries [3–6]. Compared with DBR lasers, DFB lasers are more suitable for long distance transmission due to their narrow linewidth [7–9]. In the silicon hybrid DFB laser, a Bragg grating is used for single longitudinal mode selection, which is formed by patterning a surface corrugation at the bonding interface between the III–V region and the silicon region on either the silicon surface, or III–V surface. Currently, almost all the reported hybrid DFB lasers [4, 6, 10]are using Bragg gratings which are close to the III-V active region or on the entire III-V ridge/Si waveguide. However, the expensive and time-consuming processes including e-beam lithography, material regrowth and focused ion beam et.al. must be used to fabricate the devices, which are not optimal for mass production.

To reduce the cost, a laterally coupled DFB (LC-DFB) laser with sidewall grating is proposed to simplify the fabrication process [11].Unlike the conventional DFB lasers, the grating of the LC-DFB laser is partially defined on the sidewall of the laser waveguide. In the lateral grating configuration, the sidewall grating can be simultaneously formed with the fabrication of waveguide. What's more, it is easy to achieve high grating coupling coefficient due to the large refractive index difference in the lateral grating region, which is important for short cavity DFB laser with low threshold current. However, for hybrid architectures of III-V/Si, the reported LC- DFB laser can only work with optically pumped mechanism [12].

In this paper, we demonstrate a compact electrically pumped hybrid III–V/silicon LC-DFB laser for the first time to the best of our knowledge. Third-order lateral gratings are partially made on the sidewalls of silicon waveguide through one-time patterning with the silicon waveguide by stepper lithography. A pair of vertical surface grating couplers is integrated at the two ends of the silicon waveguide for the optical coupling and characterization of the output light. Lasing emission is generated through electrical pumping into the top III-V region and optical beam is evanescent coupling into the underlying SOI waveguide, propagating in the silicon waveguide, and coupling out of the vertical surface grating coupler for wafer-scale characterizations.

2. Design and simulation

A schematic diagram of the LC-DFB grating is presented in Fig. 1, where d_{Si} indicates silicon thickness, D is ridge width, W_1 is grating lateral extension width, and Λ is the grating period.

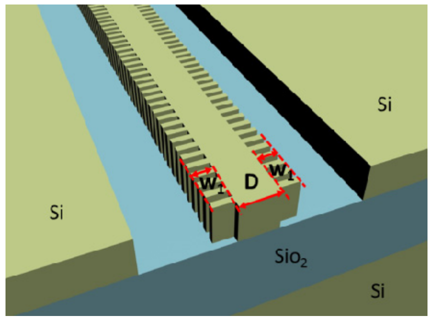

Fig. 1. Schematic diagram of the lateral coupled distributed feedback (LC-DFB) grating (without bonded III-V material on top for better illustration), the rectangles in light blue represent SiO_2 BOX layer and those in light green represent the silicon material.

An important parameter for the design and analysis of LC-DFB lasers is the grating coupling coefficient. According to the coupled-wave theory, the general expression for κ is

$$\kappa = \frac{\kappa_0^2}{2\beta} \frac{\int_{-\infty}^{\infty}\int_{-\infty}^{\infty} \Delta\varepsilon(x,y)\cdot\left|E_0(x,y)\right|^2 dxdy}{\int_{-\infty}^{\infty}\int_{-\infty}^{\infty} \left|E_0(x,y)\right|^2 dxdy} \tag{1}$$

where k_0 is the vacuum wave vector magnitude, β is the electromagnetic wave propagation coefficient, E_0 is the electric field and $\Delta\varepsilon(x,y)$ is the grating-induced dielectric perturbation [13]. By using the following derivation of the coupling coefficient formula, the formula can be written as

$$\kappa = \frac{k_0}{2n_{eff}} \left(\frac{\int_{-\infty}^{\infty}\int_{-\infty}^{\infty} n_2^2(x,y)\cdot\left|E_0(x,y)\right|^2 dxdy}{\int_{-\infty}^{\infty}\int_{-\infty}^{\infty} \left|E_0(x,y)\right|^2 dxdy} - \frac{\int_{-\infty}^{\infty}\int_{-\infty}^{\infty} n_1^2(x,y)\cdot\left|E_0(x,y)\right|^2 dxdy}{\int_{-\infty}^{\infty}\int_{-\infty}^{\infty} \left|E_0(x,y)\right|^2 dxdy} \right) \frac{\sin(\pi m\gamma)}{\pi m} \tag{2}$$

where m is the grating order. Since the refractive index distributions are generally constants in the grating regions, the above coupling coefficient calculation can be simplified using the definition of the effective refractive index and the better approximation $n_{eff,1} + n_{eff,2} \approx 2n_{eff}$. As a result [14], the formula can be reduced to

$$\kappa = \frac{k_0}{2n_{eff}}\left(n_{eff,2}^2 - n_{eff,1}^2\right)\frac{\sin(\pi m\gamma)}{m} \approx \frac{2\left(n_{eff,2} - n_{eff,1}\right)}{\lambda_0}\frac{\sin(\pi m\gamma)}{m} \tag{3}$$

where γ is the filling factor, λ_0 indicates the Bragg wavelength and the $n_{eff,1}$ and $n_{eff,2}$ are effective refractive indices from the convolution between the longitudinally-constant transverse optical field distribution and the transverse refractive index distributions in the grating slices, respectively. Here, The filling factor refers to the ratio of the length of the unetched region of the silicon waveguide to one grating period, and the $n_{eff,1}$and $n_{eff,2}$are extracted from finite element simulations in COMSOL software. A schematic drawing of the hybrid laser is presented in Fig. 2(a), and the fundamental TE mode of the hybrid laser is shown in Fig. 2(b). The confinement factor for multi-quantum wells and silicon waveguide are 6.22% and 46.72%, respectively. The reflectivity of Bragg grating can be expressed as follows [15]:

$$R = \frac{\kappa^2 \sinh^2 sL}{s^2 \cosh^2 sL + (\Delta\beta)^2 \sinh^2 sL} \tag{4}$$

where $s = \sqrt{\kappa^2 - \Delta\beta^2}$, L is the grating length, $\Delta\beta = \beta - \beta_0$ is the detuning wavevector, $\beta = 2\pi n_{eff} / \lambda$ is the average propagation constant and β_0 is the propagation constant at Bragg wavelength. In practice, an interlayer (SiO_2 or BCB) is often preferred to improve the bonding quality. Here, the interlayer thickness is considered as 10nm in the calculation.

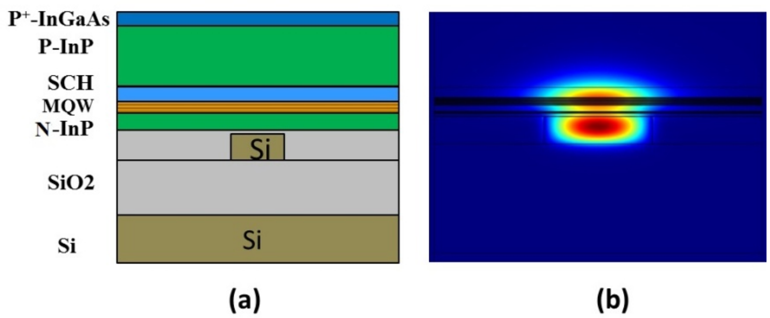

Fig. 2. (a) The Schematic diagram of the cross section of the III-V/silicon laser structure (b) and finite element simulation of fundamental TE mode for the silicon waveguide with a width of 2μm, a depth of 500nm and an interlayer thickness of 10nm.

As mentioned in the introduction part, LC-DFB structures have been realized with expensive electron-beam lithography in conventional III-V lasers [16], but it is time consuming or not preferred for large-scale fabrication. In our hybrid III-V/Si devices, the third-order (m = 3) lateral Bragg gratings are designed on silicon waveguide with the filling factor γ of 0.5. In addition, a quarter-wavelength phase-shifted region is included at the center of the silicon waveguide to break the mode symmetry in index-coupled DFB lasers. We choose the Si width as 2 μm which is for the better mode coupling into the silicon waveguide. According to the simulation, the coupling efficiency can reach about 50%, as shown in Fig. 2(b). Then we calculate the relationship between the coupling coefficient κ and the grating extension width W_1 and the result is shown in Fig. 3(a) according to formula (3) where in our calculation, d_{Si}, D, W_1, Λ and grating filling factor (with high index) are 500nm, 2μm, 1μm, 670nm, 0.5, respectively. The grating extension width is referred to the recessed width to form the lateral grating. From the result, it can be seen that κ can be easily controlled by W_1. Therefore, we choose the extension width as 1 μm for the consideration of sufficient coupling coefficient and lithography resolution.

#232468 - $15.00 USD Received 13 Jan 2015; revised 14 Mar 2015; accepted 16 Mar 2015; published 30 Mar 2015

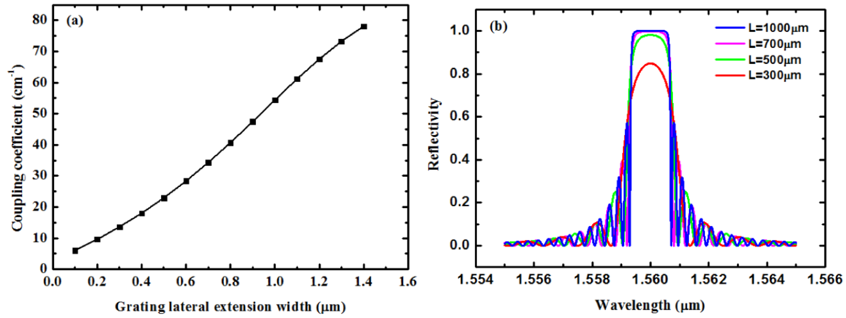

Fig. 3. (a) Relationship between the coupling coefficient and grating lateral extension width. The III-V and silicon width are chosen as 12 μm and 2μm, respectively and (b) Calculated wavelength-dependent reflection spectrum of a Bragg grating with the centre Bragg wavelength around 1560 nm in a LC-DFB structure and the grating length of 300 μm, 500 μm, 700μm and 1000μm, respectively. The structure parameters are D = 2 μm, W_1 = 1 μm, grating period Λ = 670 nm, d_{si} = 500 nm, respectively.

The calculated coupling coefficient is about 54 cm^{-1} for λ_0 = 1.56μm. The magnitude is around twice as that of conventional DFB lasers with the same grating order [13]. The reflectivity spectra of a lateral Bragg grating can be calculated according to the formula (4), and are shown in Fig. 3(b) with 300, 500, 700 and 1000 μm long lateral Bragg grating, respectively. In order to have 100% reflectance at 1.56μm and maintain short laser cavity, we choose 700 μm as our design.

3. Fabrication and results

The hybrid III-V/silicon laser is fabricated using an AlGaInAs quantum well epitaxial structure bonded to silicon waveguide with a quarter-wavelength phase-shifted lateral coupled grating. The III-V region consists of a p-InGaAs contact layer, a p-InP cladding layer (1.5μm thick), 8 AlGaInAs quantum wells (7nm) separated by 9 AlGaInAs barriers (10nm), p-type separate confinement hetero-structure (SCH, 0.18μm thick) and n-InP cladding layer (110nm) as shown in Fig. 2 (a). The asymmetric epitaxial structures are chosen for better light coupling into underneath silicon waveguide and maintain current injection efficiency at the same time.

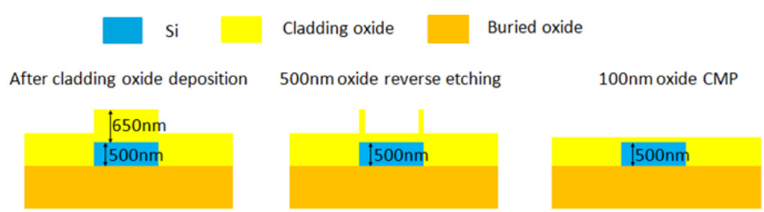

Fig. 4. Schematic diagram of planarization process, including oxide reverse etching and chemical mechanic polishing(CMP).

CMOS-compatible processes were employed to fabricate the distributed lateral-coupled grating and surface grating coupler on an 8-inch SOI wafer with 500nm silicon layer on a 2-μm BOX layer. The 500 nm silicon layer thickness is chosen for better light confinement in the silicon waveguide. The fabrication starts with the blanket silicon epitaxy from a SOI wafer with 340nm-thick silicon layer to increase silicon thickness to 500 nm, and followed by 70nm oxide deposition as the hard mask for silicon device. The surface grating coupler structure is defined by deep UV stepper photolithography and transferred onto the silicon layer by using deep Reactive-Ion-Etching (RIE) with an etching depth of 377nm. The silicon waveguide as well as the lateral grating are formed by further etching the silicon layer down

#232468 - $15.00 USD Received 13 Jan 2015; revised 14 Mar 2015; accepted 16 Mar 2015; published 30 Mar 2015

to the BOX while the surface grating couplers are protected by photoresist. Oxide cladding layer of 650nm in thickness is then deposited, followed by two planarization steps including oxide reverse etching and chemical mechanic polishing (CMP) in order to smooth the bonding surface with enhanced bonding quality. The schematic diagram of these two steps is shown in Fig. 4. The interlayer oxide thickness can be controlled by the planarization process, which leaves about 50nm oxide on top of the silicon waveguide which is limited by the CMP accuracy.

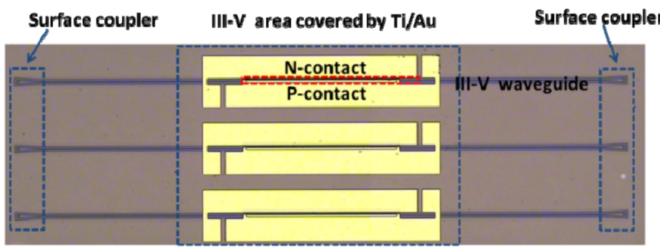

Fig. 5. Top-view optical microscope image of the fabricated silicon/III-V laser. The red dash rectangle corresponds to the part of silicon waveguide where there is processed III-V ridge on top. Take note that metal bridge would not absorb too much light with the SiO2 in between the metal and silicon waveguide.

The heterogeneous integration is achieved by means of die-to-wafer bonding. The area of each III-V die is round 9 × 9mm^2. The low-temperature bonding process starts from extremely thorough cleaning procedure for SOI wafer and III-V die wafer, respectively. Standard CMP cleaning is performed to the SOI wafer for 10 minutes in order to remove any organic contaminants. III-V wafer is cleaned in a diluted solution of NH_4OH (NH_4OH: DI water = 1:15) for 1 minute. Then both wafers are undergone O_2 plasma surface activation for 60 seconds in a RIE chamber. After that de-ionized water rinse cleaning is performed to terminate the surface with –OH groups for both wafers. The bonded pairs are then placed into an EVG bonder with 1000N mechanic force for 3mins, followed by low temperature annealing at 300 °C for 15 hours. As the bonding is made between the III-V die and SOI wafer and their sizes are relatively large, it is believed that the bonding thickness is uniform enough to maintain the strong κ of the lateral grating for the small area of the processed hybrid laser. After InP substrate removal with HCl and water mixture solution, 12μm wide mesa are formed by photolithography, followed by mixture of H_3PO_4, $H_2O_2$and HCl to etch InGaAs contact layer and p-InP cladding layer, respectively. Finally, the etching stops on the surface of n-InP cladding layer by etching SCH layer and quantum wells layer using H_3PO_4:H_2O_2:H_2O solution again. Then a layer of SiO_2 insulator with the thickness of 300nm is deposited and both 4μm p-type and 10μm n-type injection windows were formed by one-time photolithography followed by HF solution to etch SiO_2. After that, Ti/Au metal contacts are made by sputtering. Finally, separation slots are formed between the N- and P- contact by wet etching of Ti/Au using diluted HF and KI solution, respectively. The device after the fabrication is shown in Fig. 5. Although there is metal bridge crossing the top of the silicon waveguide, less light in silicon waveguide will be penetrated to the Ti/Au metal layer due to the existing 300 nm SiOx layer according to the index difference. The calculated loss coefficient due to the top 20 μm metal is estimated as 0.037/cm for the fundamental mode in silicon waveguide. The grating has the same length with III-V ridge, and is directly located beneath III-V region. The length for silicon waveguide and III-V ridge are about 2500 and 700μm, respectively. Figure 6 shows the top-view scanning electron micrograph (SEM) of the fabricated lateral grating and surface coupler on SOI. As shown in Fig. 6, the grating period and surface coupler period are about 670nm and 640nm, which match well with our theoretical design. The area of each surface coupler is about 15 × 15μm^2. The details are illustrated by part magnification as shown in Fig. 6(c) and 6(d). It can be seen that the sidewalls of the grating are very smooth and steep. Although the 2μm wide silicon waveguide indeed is not a single mode waveguide, the light is generated from the III-V part and the III-V width is chosen as 12 μm for the ease of the fabrication. Hence a relatively wider silicon waveguide is chosen for better coupling the light into the silicon waveguide. High order modes may exist for wide silicon waveguide, but they can't lase due to the higher modal loss than the fundamental mode. We also conduct simulations on the effect of misalignment between the center of III-V ridge and Si waveguide. The result shows that even for a large misalignment of 3μm the mode profile and confinement factor in MQW as well as Si waveguide remain almost unchanged. Such a large misalignment can be well controlled within the photolithography fabrication resolution. However, there is a waste of current injection efficiency which is caused by such wide III-V ridge. For future batches, the III-V ridge should be narrowed to improve the efficiency and reduce the consumed power, which is significant for the real applications.

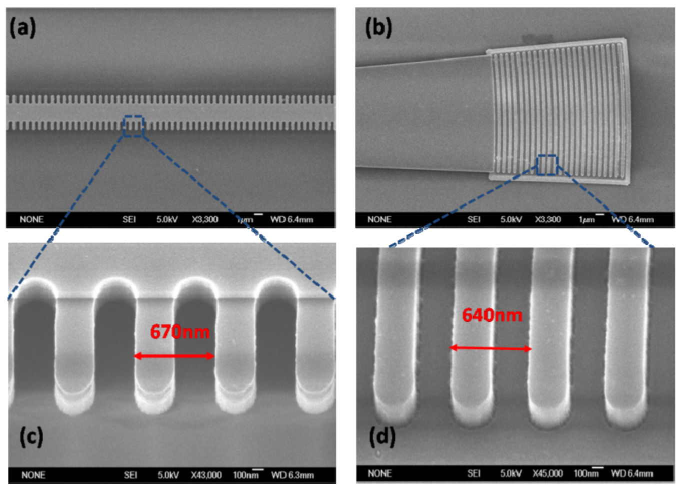

Fig. 6. The scanning electron microscope (SEM) image of (a) the Bragg grating, and (b)surface coupler ; (c) and (d) are the respective images of (a) and (b) in magnification.

The laser beam output is collected through one surface grating coupler by a fiber and then characterized by using both a spectrum analyzer and an optical power-meter. The P-I curve and spectra are measured under the pulsed mode operation at room temperature (20 °C), as shown in Fig. 7(a) and 7(b), respectively. To increase the coupling efficiency of surface coupler, the light is collected by the fiber inclined at 8 degree from the normal line to the chip surface. A single-mode emission is observed in the lasing spectrum, and the peak wavelength is about 1.56 μm and side mode suppression ratio (SMSR) is larger than 20dB as shown in Fig. 7(b). As shown in the P-I curve, the threshold current is about 130mA, and the corresponding threshold current density is about 1.54kA/cm^2. For the given structure, the expected threshold current density is largely dependent on the coupling strength κL. The detailed calculation result for the theoretical threshold current under different coupling strength is shown in Fig. 8 with a fixed cavity length of 700 μm. The calculation assumes there is no reflection from the surface coupler at the both ends, like the conventional DFB laser with AR coatings on the both facet. It is found that strong coupling strength will lead to a relative low threshold current. With the current κL of 3.78, the calculated threshold current [17] is ~90 mA with the injection efficiency, material gain and transparent carrier density are set as 0.6, 1500 cm^{-1} and 1x10^{18} cm^{-3}, respectively, which is much smaller than measured threshold current. The thick oxide interlayer in the device structure led to the high threshold current as shown in [18]. In our case, the residual oxide thickness (about 50nm) after CMP could not be controlled accurately, which may be larger than 10 nm from our design, and this largely reduces the portion of light coupled into silicon according to the simulations as well as the coupling strength. Therefore, the low optical confinement in SOI waveguides of the current devices limits the performance of grating, and then resulted in a small SMSR. It is believed that by optimizing the structure such as adopting the taper design to enhance the coupling efficiency [5] and reducing the interlayer SiO_2 thickness in the real fabrication process, the device performance would improve significantly.

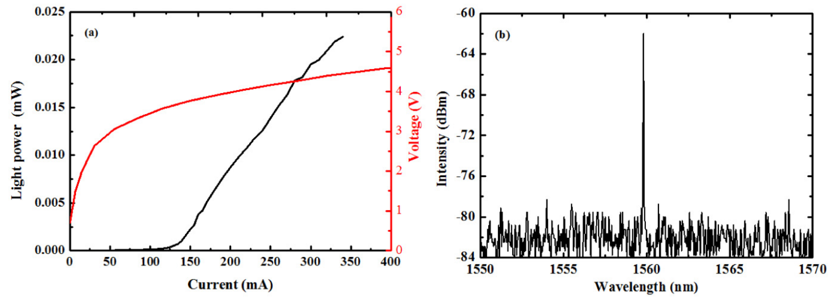

Fig. 7. (a) Measured light power output versus injection current from one surface coupler withthe calibration of surface couplers and waveguide losses and (b) The laser spectrum under pulsed operation with 1% duty cycle at the injection current of 200mA.

Besides the reduced coupling strength κL [19], the low optical power is also due to the relatively high loss from the surface coupler, grating scattering and bonding interface non-radiative recombination [20], among which the surface coupler loss plays a dominate role as mentioned above. The pure optical loss from the surface coupler and waveguide is measured without any III-V materials on SOI for calibration purpose. During the measurement, one surface coupler serves as the input and the other one as the output. The measured total optical loss is about 20dB/coupler, which is larger than we expect. One reason is the non-optimized parameter design for the surface coupler such as the grating depth and period, etc. In addition, polarization sensitivity of the surface coupler can also cause additional optical loss [21]. Due to the constraints of measurement setup, the measurement could not be integrated with temperature-control stages and the measurement has to be done at room temperature. 0.022mW calibrated output power is the power from one surface coupler if there is no optical loss in the two surface couplers and sidewall gratings, as shown in Fig. 7(b). We will improve the surface coupler design such as the etching depth, filling factor and periods etc. to improve the output power in the next step. Mode converters between the hybrid waveguide and the silicon passive waveguide can also be integrated on the front and rear end of the cavity of our device to further improve the output power.

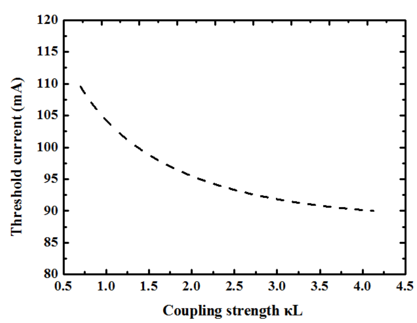

Fig. 8. Calculated threshold current vs. different coupling strength κL if there is no reflection from the surface coupler. The injection efficiency, material gain and transparent carrier density are set as 0.6, $1500cm^{-1}$ and $1x10^{18}$ cm^{3}, respectively. Cavity length is 700μm long. For comparison, the measured threshold current is ~130mA, which is much higher than the expected value of ~90mA.

4. Conclusion

In conclusion, we demonstrated a hybrid III-V/silicon laser with laterally coupled grating patterned on 500nm -thick SOI platform. A pair of surface couplers is integrated at the two ends of silicon waveguide to characterize the device performance. The measured threshold current density is 1.54kA/cm^{2}which is larger than calculated value and a single mode operation with a SMSR larger than 20dB is achieved. The main reason for the limited performance comes from the limited interlayer thickness control and surface coupler dimension, which increases the threshold current, reduces the SMSR and the output power. It might be safe to say this demonstration serves as a proof-of-concept, and the performance would improve significantly with the optimized design and fabrication.

Acknowledgment

This work is supported by A*STAR SERC Future Data Center Technologies Thematic Strategic Research Programme under Grant No. 1122804038, and A*STAR – MINDEF Science and Technology Joint Funding Programme under Grant No. 1223310076.

#232468 - $15.00 USD Received 13 Jan 2015; revised 14 Mar 2015; accepted 16 Mar 2015; published 30 Mar 2015